Drag Coefficient for a Circular Obstacle in a Quasi-Two-Dimensional Dilute Supersonic Granular Flow

J. F. Boudet and H. Kellay

Université Bordeaux 1, Centre de Physique Moléculaire Optique et Hertzienne, CNRS UMR 5798,
351 cours de la Libération, 33405, Talence France

The measurement of the drag coefficient of a dilute granular flow around a cylinder is carried out over a wide range of Knudsen numbers. The variation of this coefficient shows a smooth transition from a freely falling grains regime to a continuous flow regime. This is reminiscent of the behavior of gases in the supersonic regime. This transition is accompanied by remarkable changes of the density and velocity profiles near the cylinder. A simple model is proposed for the transition regime which is in agreement with the experimental measurements.

Granular flow around obstacles has received much attention in recent years. This flow evolves with the density of incoming particles from a situation where the grains fall individually on the obstacle to a situation where dense patterns form as displayed in Fig. 1. These changes are related to shock formation [1,2] since the "sound velocity" of flowing and dilute assemblies of grains can be much smaller than the flow velocity [3,4] allowing detailed laboratory studies of supersonic flows around obstacles. A pressing question is the force exerted by the flow on the obstacle. This is important for different fields such as geophysics, the processing of diverse granular materials, and the control of avalanches through placing protection barriers for example [5]. This question has received much attention, in the dense flow regime, both experimentally and numerically [6–8] but has received little attention from experimentalists in the dilute regime [8,9].

The case of a dilute granular flow around a cylinder studied here shows two different regimes for the variation of the drag coefficient versus the so-called Knudsen number k_D which compares the mean free path in the gas to the dimensions of the object. The transition between these two regimes occurs smoothly and mimics the variation observed for molecular gases [10,11]. One of the main observations concerns notably this transition regime between the dilute and more dense case. Our results show that it is characterized by quantitative changes of the density and velocity profiles around the cylinder and a simple model is proposed to account for the transition regime. Our experiments bring new insight and new information for the granular kinetic theory, for which much progress has been achieved in the past decade [12], by providing, in a simple experiment, crucial elements for the transition from very dilute to dense flows.

Here we focus on the drag force exerted on a thin cylinder by a dilute vertical flow of grains confined between two glass plates so that the situation is quasi-two-dimensional allowing accurate flow visualizations. The velocity of the flow is near 200 cm/s giving a flow Mach number near 8 [1,4]. The obstacle sits on top of a balance so that the exerted force can be measured during the experiment. We set the thickness of the obstacle (6 mm) slightly smaller than the distance between the two plates ($h = 6.5$ mm). The spacing left is smaller than 1 grain diameter so that the beads cannot get lodged in this spacing leaving the obstacle free to move in the vertical direction. A flow of grains then impacts the cylinder. During the flow, the mass weighed by the balance is non zero with a stable value when the flow reaches a steady state. It is this constant value which we record for each flow rate. In this manner, we record the variation of the exerted force ($F = mg$ where m is the measured mass and g the acceleration due to gravity) versus the incident flow volume fraction ϕ_a measured before the incident flux interacts with the obstacle using either the known flux or a method developed in [1]. This fraction was varied through the variation of the incident mass flux by fixing a variable gate at the entrance of the flow. This procedure therefore allows us to produce the canonical curve: drag coefficient versus Knudsen number. The two quantities are defined in the following manner: $C_d = \frac{F}{\frac{1}{2}\rho\phi_a V_a^2(D+d)h}$ and $k_D = l(\phi_a)/D = \frac{d}{6\sqrt{2}\phi_a D}$.
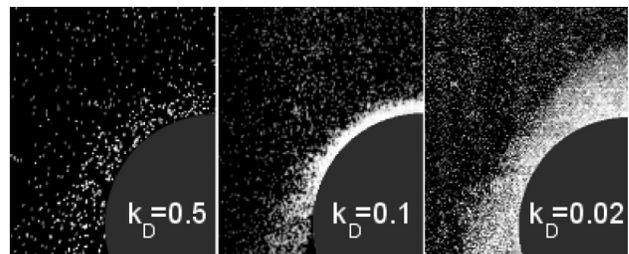
FIG. 1. Pictures of the flow of grains around a cylindrical obstacle sandwiched between two transparent vertical plates for three different flow volume fractions or Knudsen numbers (steel spheres of $d = 1$ mm and aluminum cylinder of $D = 11$ cm). Note that as k_D decreases, the density in the close proximity of the cylinder increases considerably going from the dilute limit at $k_D = 0.5$ to the dense limit at $k_D = 0.02$.

Here, ρ is the density of the particles, V_a is the velocity of the flow measured using particle tracking, D is the diameter of the cylinder, d is the diameter of the grains, and $l(\phi_a)$ is the mean free path.

In the high k_D limit ($k_D > 1$), C_d is expected to asymptote to a constant value given by $C_d = \frac{4}{3}(e + 1)$ [9], where e is the inelasticity coefficient of the grains with the obstacle ($e = 0.93$ for steel spheres). This is borne out experimentally as shown in Fig. 2(a), where the measured force varies linearly with the volume fraction with the expected slope as shown by the solid line. This regime corresponds to the free particle flow. As ϕ_a increases, the force deviates from the expected result indicating the onset of a reduction in the value of C_d for $k_D < 2$ as has been observed in numerical simulations [9]. The initial decrease of C_d with k_D can be understood in a simple way: for high k_D, the grains fall individually on the obstacle and, after colliding with the obstacle, rebound (specular reflection) exchanging momentum with the obstacle. As the number of incident grains increases (and therefore as k_D decreases), the momentum transfer to the obstacle decreases as part of the flow is diverted in the downward direction (see Fig. 1) due to multiple grain-grain and grain-obstacle collisions leading to a reduction of C_d.

For even higher volume fractions, the accumulation of grains on top of the obstacle introduces an additional force on the obstacle: the weight of the dense zone. To take this into account, we have carried out visualizations of the flow near the obstacle, estimated the area of the dense zone and evaluated its weight. An implicit assumption in the evaluation of the mass of the dense zone is that its average volume fraction is constant and varies negligibly with the incident volume fraction as has been verified previously through measurements of the volume fraction profiles of this zone [1]. *A priori*, the measured force should be the

sum of this weight and the drag exerted by the flow. Figure 2(b) summarizes our data. Note that as expected, the force increases slightly faster than the weight of the dense zone at first but as the flux increases, the force becomes smaller than the weight. This surprising behavior is at first irreconcilable with the simple assumption that the weight and the drag should just add up. In order to explain this, we have to invoke a Jenssen like effect associated with the presence of the vertical walls confining the flow. Let us recall the simple case of a grain filled vertical silo. For this case, the apparent mass of the grains, measured at the bottom of the silo, is a linearly increasing function of the height of the grains, i.e., their mass in the silo. The measured mass then saturates for higher heights giving an apparent mass smaller than the mass enclosed in the silo. This effect has been documented in different experiments and the expression for the apparent mass of the silo deduced and explained through taking into account the friction of the grains on the walls of the silo [13]. The apparent mass can be written as $M = M_{\text{sat}}(1 - \exp(-M_{\text{silo}}/M_{\text{sat}}))$, where M_{sat} is the mass at saturation and M_{silo} is the enclosed mass. If we invoke a similar effect here, for $k_D < 0.1$ for which the accumulated mass becomes non negligible, we need to take into account the additional force induced by the flow, the drag force sought after here. In this case, the expression for the force was derived in [14] for the case where an additional weight was placed on top of the pile enclosed in the silo. This expression can be adapted to our case by simply replacing the additional weight by the drag force and obtain $F = (C_d Q - M_{\text{sat}} g) \times \exp(-M_{\text{pattern}} g / M_{\text{sat}} g) + M_{\text{sat}} g$. Here $C_d Q$, ($Q = \frac{1}{2} \rho \phi_a V_a^2 (D + d) h$), is the drag force exerted by the flow. The two unknowns are the value of C_d and the value of M_{sat}. Figure 2(b) plots our data along with the values deduced from the expression for the full force exerted by the drag and the additional mass. The best fit gives $M_{\text{sat}} g = 1250$ mN and 300 mN for steel and glass beads respectively; the difference in value between glass and steel spheres is due to the difference in the mass density of the two materials. From this curve, we obtain the drag coefficient in the low k_D limit. Figure 3 shows the variation of C_d versus k_D. Note that the trend of decreasing C_d as k_D decreases below 2 is confirmed down to very small values where the drag seems to saturate at a value of about 1.

Measurements of the vertical velocity profile $V_y(z)$ (using particle tracking) and the volume fraction profile $\phi(z)$ (using a method developed in [1], z is the distance from the center of the cylinder) near the cylinder for different ϕ_a, see Fig. 4, allow us to make an independent estimate of C_d by estimating the flux of momentum across a chosen section. The difference between the incoming momentum flux and the outgoing momentum flux gives $C_d = 2\rho h[\phi_a V_a^2 L - \int_0^L \phi(z) V_y^2(z) dz]/Q$, where L is a large distance extending far away from the cylinder wall. This estimate of C_d is shown in Fig. 3. The values of C_d turn out to be in good agreement with those estimated from the
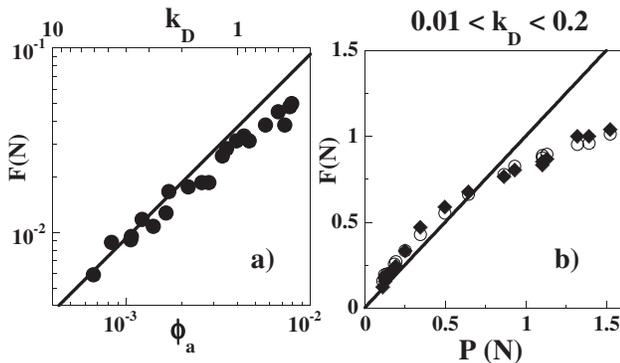
FIG. 2.   (a) Force versus ϕ_a for the high k_D range for which the mass of accumulated grains on top of the cylinder is negligible. The solid line is the expected result for a constant C_d. (Steel spheres of $d = 1$ mm and a cylinder of $D = 2.7$ cm) (b) Force versus the weight of the dense zone on the obstacle for the low k_D range. (Steel spheres of $d = 1$ mm for $D = 11$ cm). Open symbols are measurements, closed symbols are obtained using the model in the text.
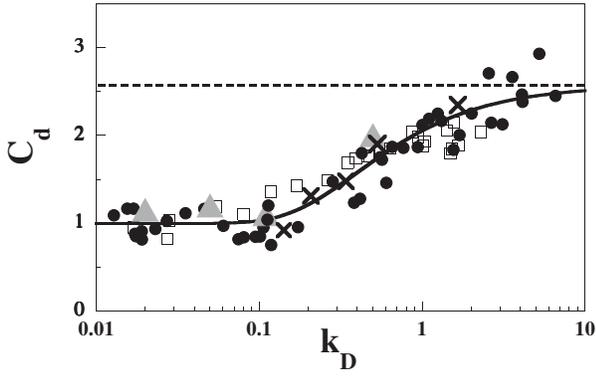
FIG. 3. C_d versus k_D (solid circles: steel spheres $d = 1$ mm, $D = 11$ cm and 2.7 cm, squares: glass beads $d = 1.2$ mm and $D = 11$ cm, triangles: estimates from momentum flux difference, crosses: estimates from integrating the pressure around the cylinder). The horizontal dashed line is the expected result for high k_D. The solid line is the best fit using the proposed model.

force measurements validating our analysis of the effect of the additional weight due to the accumulation of grains. This agreement also suggests that the effect of shear stresses is small. In addition to these considerations, we have made an attempt at evaluating the drag by integrating the pressure around the cylinder. This procedure requires the use of an expression for the pressure of the granular gas around the cylinder [1]. The values of C_d extracted from such a calculation of the pressure (the local density and the local temperature were determined all around the cylinder) turn out to be in good agreement with those obtained from the force measurements and the control volume method, as shown in Fig. 3, indicating that the drag is dominated by pressure drag.

The trend obtained here for C_d versus k_D bears great resemblance to that obtained for supersonic gas flows around a cylinder for which the high k_D plateau has been attributed to diffuse reflection of the molecules on the obstacle in the free molecular flow limit and the lower plateau at low k_D to the continuum flow limit [10]. The transition from the first to the second regime is smooth just like for gases. This is our main result since it shows that granular gases and molecular gases behave similarly as far as drag is concerned despite the obvious differences between the two systems. The transition region between the two regimes remains an open problem is gas flows. Can this region be better understood for granular flows?

First and since the two limiting values are well defined, the transition region from the first regime to the second regime can be obtained. The solid line in Fig. 3 is a fit to a simple model which assumes that the probability for a particle to travel a distance x without suffering a collision is simply $\exp(-\frac{x}{l(\phi_a)})$. This simple model assumes that particles exit the interaction zone (between the flow and the cylinder) if they do not undergo a collision over a distance of roughly one cylinder radius. These particles contribute, on average, a factor C_d corresponding to the
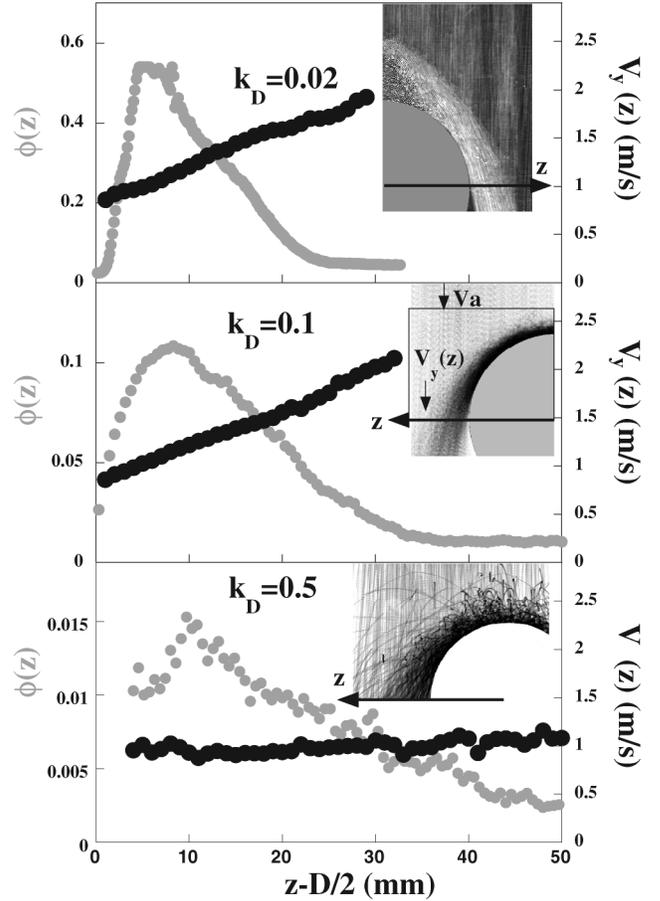
FIG. 4. Volume fraction (gray dots) and vertical velocity (black circles) profiles measured at mid level of the cylinder for different ϕ_a. Measurements are along the z axis with origin at the center of the cylinder. The insets show representative illustrations of the flow. For small k_D, the flow is dense while for the higher k_D (0.5) the flow is less dense with particles rebounding away from the obstacle.

high k_D limit. The rest of the particles are trapped near the obstacle and contribute to the continuous flow with a C_d corresponding to the low k_D limit. The expression for C_d using these considerations becomes $C_d(k_D) = C_d(k_D \to \infty) \exp(-\frac{1}{2k_D}) + C_d(k_D \to 0)(1 - \exp(-\frac{1}{2k_D}))$. Here the characteristic distance x used is the radius of the cylinder. Actually the best fit gives a value of $D/2.5$. The solid line in Fig. 3 shows that these considerations capture the essential features of the variation of C_d versus k_D.

Second, the structure of the flow around the cylinder actually changes as the transition region is approached as shown in Fig. 4. We noted two remarkable features. For $k_D > 0.5$, the velocity profile is relatively flat while the volume fraction is small with a wide profile. For $k_D < 0.1$, the flow is well established with a clear velocity profile and volume fraction profile (which reaches high values near 0.55 near the cylinder for low k_D). The velocity profile shows a well defined shear rate linking a velocity at the cylinder wall (which is roughly the free fall velocity of a
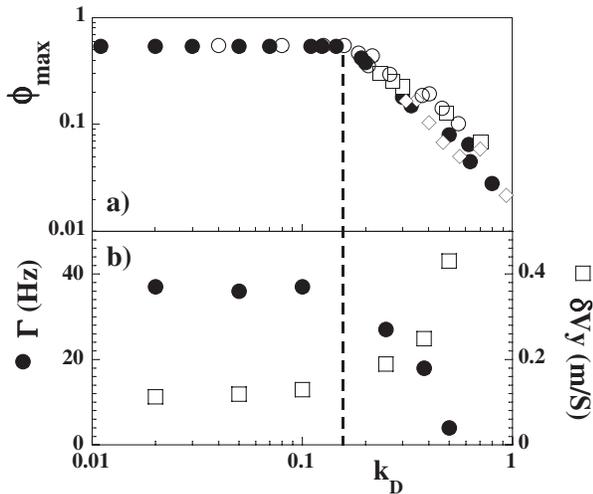
FIG. 5. $\phi_{\max}$ on top of the obstacle, shear rate Γ and the standard deviation of the vertical velocity δV_y near the mid level of the cylinder versus k_D for steel spheres. Note the changes occurring near $k_D = 0.15$. Upper graph: the closed symbols are for steel spheres while the open symbols are for glass beads (squares and diamonds: different D but fixed ϕ_a, circles: varying ϕ_a and fixed D).

particle starting with a zero velocity near the summit of the cylinder) to the outer velocity (the free fall velocity of incident particles). Changes in the structure of the flow versus k_D are summarized in Fig. 5. Here we show the changes occurring for the maximum volume fraction, shear rate and velocity fluctuations as k_D changes. Indeed, this figure shows that the maximum volume fraction on top of the obstacle reaches a plateau value near the random loose packing fraction of 0.55, that the shear rate at mid height near the cylinder reaches a constant value, near 38 s^{-1}, and the fluctuations in velocity (the standard deviation) decrease to a constant level for $k_D < 0.1$. For $k_D > 0.1$, the volume fraction on top of the obstacle and the shear rate decrease but the fluctuations increase. For $k_D > 0.5$, the velocity profile becomes flat with a barely measurable shear rate while the fluctuations in velocity increase and the volume fraction continues to decrease. The fluctuations in velocity in this regime reflect the fact that the flow is not dense and that individual particles that rebound at different locations on the obstacle arrive at the measurement position with different speeds. The characteristics described above delimit the three different regions illustrated by our measurements of C_d: the free particle flow, the continuum like flow and the transition region. For high ϕ_a ($k_D < 0.1$) the flow is continuous with a well defined velocity profile, a small fluctuation level, and the formation of a large density zone on top of the obstacle (reminiscent of a stagnation zone). For very low ϕ_a, the flow is dominated by single particles colliding with the obstacle. The transition region for $0.1 < k_D < 1$ is characterized by the continuous variation of the shear rate and maximal density. The drag curve

therefore signals a transition from a discrete situation to a continuous situation as has been remarked for the case of supersonic gases flowing past a cylinder. Our results bring new information as to how this transition occurs for the granular case: it occurs smoothly with the gradual establishment of a well defined linear velocity profile, with a well defined shear rate, and a well-defined density profile.

In conclusion, we have carried out measurements of the drag coefficient versus the flow Knudsen number for a wide range of flow densities in the case of a cylinder in a granular flow. The drag coefficient has two limiting values at high and low Knudsen numbers and shows a smooth transition as this parameter varies. This behavior is reminiscent of that of supersonic gases flowing past a cylinder. The variation of the drag is related to the flow structure around the cylinder and its evolution with flow volume fraction brings new insight into the interaction of a supersonic flow with an obstacle. Remarkable changes in the velocity profiles and density profiles occur as the flow crosses over from the very dilute regime to the more dense regime. A simple model is proposed to extrapolate between the two regimes and capture the essential features of the transition region.

[1] J.-F Boudet, Y. Amarouchene, and H. Kellay, Phys. Rev. Lett. **101**, 254503 (2008).
[2] Y. Amarouchene, J. F. Boudet, and H. Kellay, Phys. Rev. Lett. **86**, 4286 (2001).
[3] E. C. Rericha et al., Phys. Rev. Lett. **88**, 014302 (2001).
[4] Y. Amarouchene and H. Kellay, Phys. Fluids **18**, 031707 (2006).
[5] T. Faug, R. Beguin, and B. Chanut, Phys. Rev. E **80**, 021305 (2009).
[6] R. Albert et al., Phys. Rev. Lett. **82**, 205 (1999).
[7] D. Chehata, R. Zenit, and C. R. Wassgren, Phys. Fluids **15**, 1622 (2003).
[8] A. Levy and M. Sayed, Phys. Fluids **19**, 023302 (2007); A. Levy and M. Sayed, Powder Technol. **181**, 137 (2008).
[9] C. R. Wassgren et al., Phys. Fluids **15**, 3318 (2003); R. Bharadwaj, C. R. Wassgren, and R. Zenit, Phys. Fluids **18**, 043301 (2006).
[10] G. J. Maslach and S. A. Schaaf, Phys. Fluids **6**, 315 (1963).
[11] C. Cercignani, Rarefied Gas Dynamics: From Basic Concepts to Actual Calculations (Cambridge University Press, Cambridge, England, 2000).
[12] M. H. Ernst and R. Brito, Granular Gas Dynamics, edited by T. Poeschel and N. Brilliantov, Lecture Notes in Physics Vol. 624 (Springer-Verlag, Berlin-Heidelberg-New York, 2003).
[13] Y. Bertho, F. Giorgiutti-Dauphiné, and J.-P. Hulin, Phys. Rev. Lett. **90**, 144301 (2003); G. Ovarlez and E. Clément, Europhys. J. E **16**, 421 (2005).
[14] J. Duran, Sables, Poudres, et Grains (Editions Eyrolles, Paris, 1997).